SUPPLEMENTARY FIGURE LEGENDS

Supplementary Figure 1: Directed differentiation of HESCs to NPCs displays extensive DNA demethylation within chromatin accessibility loci. (A) Transcript expression as determined by RNA-seq is shown for canonical ESC and NPC markers. The displayed data represents the average *FPKM* normalized read counts for two biological replicates. (B) Library complexity was calculated using *preseq* for each sequencing library. The number of distinct reads for the sample is displayed. (C) Correlation between biological ATAC-Me replicates was calculated to evaluate reproducibility across replicates using *multiBigWigSummary*. The data points and Spearman correlation coefficient for each comparison is plotted. (D) Correlation between biological RNA-seq replicates was calculated to evaluate reproducibility across replicates using *multiBigWigSummary*. The data points and Spearman correlation coefficient for each comparison is plotted. (E) Static ChrAcc regions over the time course were identified using *TC-seq* (dynamic n = 38189, static n = 63026, $|\log_2\text{-fold}| > 2$, adjusted p-value < 0.05). *deeptools* is used to display the ChrAcc and DNAme values of these static peaks at all time points. Regions are sorted by decreasing normalized read count signal intensity at the 0-hour time points and are consistent across all heatmaps. Regions are scaled relative to each other along the center of each heatmap with the up and downstream flanking region (Methylation = +/-1kb, Accessibility = +/-0.5kb) . Related to Figure 1.

Supplementary Figure 2: Unsupervised clustering of chromatin accessibility reveals temporally distinct regulatory groups with divergent changes in enhancer states. (A) The *factoextra* package was used with the “wss”, “silhouette”, or “gap_stat” methods to calculate the total within-cluster sum of square, the average silhouette of observations, or the estimated gap statistic, respectively, for 1-20 clusters to inform the C-means cluster number for TC-seq. (B) Gene ontology enrichment was performed on genes associated with any dynamic cluster region using GREAT with the default, basal plus extension method of association. Ontology is grouped

by dynamic cluster though there was no significant enrichment for regions contained in *Early Transient* and *2-day Transient* clusters (padj <0.05). The dot plot represents enrichments across biological processes, molecular function, and cellular component analyses. (C) Gene ontology enrichment was performed on genes associated with accessible regions using GREAT for biological processes. Ontology is grouped by accessibility behavior, static versus dynamic. The top 10 most significant processes are shown for dynamic regions, while all processes passing the significant threshold (padj <0.05) are displayed for static regions due to lower enrichment. (D) Annotation of regions by chromatin state was performed using the chromHMM[32] 18-state annotations from HESCs and NPCs. A Sankey plot displays the change in the regions' chromatin state from the ESC to NPC stages. *Gradual Opening* and *Late Opening* were consolidated for this visualization. (E) A Sankey plot displays the change in chromatin state for *Gradual Closing* and *Delayed Closing* which were consolidated for this visualization. (F) Histograms represent the distribution of observed/expected CpG ratio for regions contained in each accessibility cluster. The mean of all regions is included for all clusters. The ratio is calculated as follows: $Number\ of\ CpG * N\ /\ (Number\ of\ C\ *\ Number\ of\ G)$, where N = length of the region. (G) Average Obs/Exp CpG ratios were calculated for each major ChrAcc trend, with the distribution of regional values shown by violin plot. Mann Whitney U test was performed for individual comparisons to the *Transient* regions (*Transient vs. Closing* p-value = 4.507e-8, *Transient vs. Opening* p-value <2e-16, *Transient-Static* p-value <2e-16). Related to Figure 2.

Supplementary Figure 3: DNAme dynamics are unidirectional and temporally discordant with chromatin accessibility. (A) Line plot of the standardized difference of the mean across the time course for all dynamic loci, one standard deviation from the mean is shown by gray ribbon. Standardized difference of the mean across time was calculated for the average regional DNA methylation state of dynamic accessible fragments. (B) Boxplots display the change in average methylation values across regions between the first (0 day) and last (12 day) timepoints.

Regions are grouped by their accessibility behavior. (C) Violin plots display the distribution of regional methylation values for all accessible regions in each methylation cluster. Methylation clusters were defined by hierarchical clustering using the *ward.D2* clustering algorithm. 25,964 stably hypomethylated regions displaying <10% 5-mC across all time points are not displayed. (D) Scatterplots display methylation measurements of CpG sites within ChrAcc peak regions quantified by ATAC-Me or 6-base sequencing. (E) Boxplots display the standard difference of the mean across time for ChrAcc and gene expression. Standardized differenced was calculated using $\log_2$(normalized ATAC read counts +1) and $\log_2$(normalized read counts+1) of neighboring transcripts (top 25% most variable). Lines represent median values. Related to Figure 3.

Supplemental Figure 4: Discordant DNAme patterns generate historical hypomethylation records. (A) Normalized read counts for three JASPAR POU family root members, POU5F1, POU3F1, and POU3F2, derived from RNA-seq data captured at each timepoint. Data was normalized for sequencing depth using FPKM at each timepoint. (B) Average regional methylation and accessibility (C) for all TF binding sites that were called as bound or unbound by TOBIAS. Binding site regions included the TF motif sequence +/-50 bp. Accessibility signal is displayed as the $\log_2$ transformed ATAC signal. ATAC-Me read count was normalized using DESeq2 prior to transformation. (D, E) Line plots show average methylation values over time visualized by TF binding behavior. Methylation values are averaged across CpGs contained in the TF motif +/-50bp. The annotated time represents the time point of the TF binding event, or the time point at which a motif transitions from being bound to unbound (lose events, D) or vice versa (gain events, E). Shaded ribbons represent one standard deviation above or below the mean methylation. Related to Figure 4.

Supplementary Figure 5: Early and sustained accumulation of 5-hmC demarcates demethylation timing at lineage specifying enhancers (A) Heatmap displaying transcript levels for TET family members and the TET2 binding partner CXXC4/IDAX normalized using

FPKM. Values were log_2 transformed prior to plotting and each transcript expression is scaled across the time course using the z-score. (B) Gating parameters were applied at each timepoint to capture single cell events within each stage of the cell cycle. Representative gating for one biological replicate is shown. Axes represent signal intensity and are labeled according to the channel being visualized. (C) Representative histograms of median fluorescent intensity for 5-hmC signal across cell cycle stages as measured by flow cytometry, produced in Cytobank. Histograms colors represent the transformed ratio relative to the minimum within the displayed representative sample. (D) Boxplots display the standard difference of the mean across time for DNA methylation, chromatin accessibility, and 5-hmC. Standardized differenced was calculated using log_2(normalized ATAC read counts +1) the average fraction 5-mC of the chromatin accessible DNA fragments, and the average fraction 5-hmC of accessible peak regions. Lines represent median values. 6-base data for three timepoints (0, 4 and 8 days) is displayed alongside ATAC-Me data for the timepoints closest to 6-base timepoints (0-day, 4.5-day, 6-day, and 12-day). (E) Change in mean 5-hmC proportion for accessibility clusters not displayed in Figure 5G. Regional means are averaged across all regions contained in the cluster. “Total” represents the difference between 8-day and 0-day data, “0-4 day” represents the difference between 4-day and 0-day data, and “4-8 day” represents the difference between 8-day and 4-day data. (F) The histogram displays the distribution of average regional 5-hmC fraction across all dynamic regions. (G) Aggregate profiles display 5-mC signal at TF footprints for a JASPAR root cluster containing BHLHA15. TF footprinting and binding state designation was performed using TOBIAS. Profiles display signal at footprint sites with a flanking distance of +/-1000bp, binned into 25bp bins. Related to Figure 5.

Supplementary Figure 6: Chromatin accessibility prediction by machine learning. (A) Diagram of timepoints sampled by ATAC-Me and 6-base methylation data assays used for machine learning models. ATAC was measured at 0, 4.5, and 12 days. 5-mC along with 5-hmC

was assayed at 0, 4, and 8 days with 6-base sequencing. (B) Schematic of machine learning model workflow. A BED file representing enhancers, promoters, static accessibility regions, or dynamic accessibility regions was used as input for prediction targets. Training and testing datasets were split on chromosome 1. Training was performed on regions from all chromosomes withholding chr1, and testing was performed on chr1 regions. Input for training data consisted of methylation levels at individual CpG sites measuring 5-mC, 5-hmC, or both from 6-base sequencing data performed at 0, 4, or 8 days. Models were subsequently tested on ATAC data derived from 0, 4.5, or 12-day datasets. (C) Dot and line plots of spearman ρ values of XGBoost models trained across the same three methylation data combinations. Models were similarly trained on the methylation of one day and tested across all three timepoints. Input data for models were subdivided into enhancers or promoter regions. Model performance by input methylation datatype is distinguished by line color. (D) Bar plots of spearman ρ values (predicted vs. expected accessibility) for static region models trained on methylation values from 0, 4, or 8-day data and tested to predict accessibility at 0, 4.5, and 12 days. (E) Bar plots of spearman ρ values (predicted vs. expected accessibility) for dynamic region models trained on 0-day data. (F) Scatter plots display the observed accessibility versus the predicted accessibility for models trained and tested on 0-day data across either dynamic or static accessibility regions. Dotted lines are defined by the slope between the points [minimum predicted value, minimum predicted value] and [maximum predicted value, maximum predicted value] in each scatterplot. Related to Figure 6.

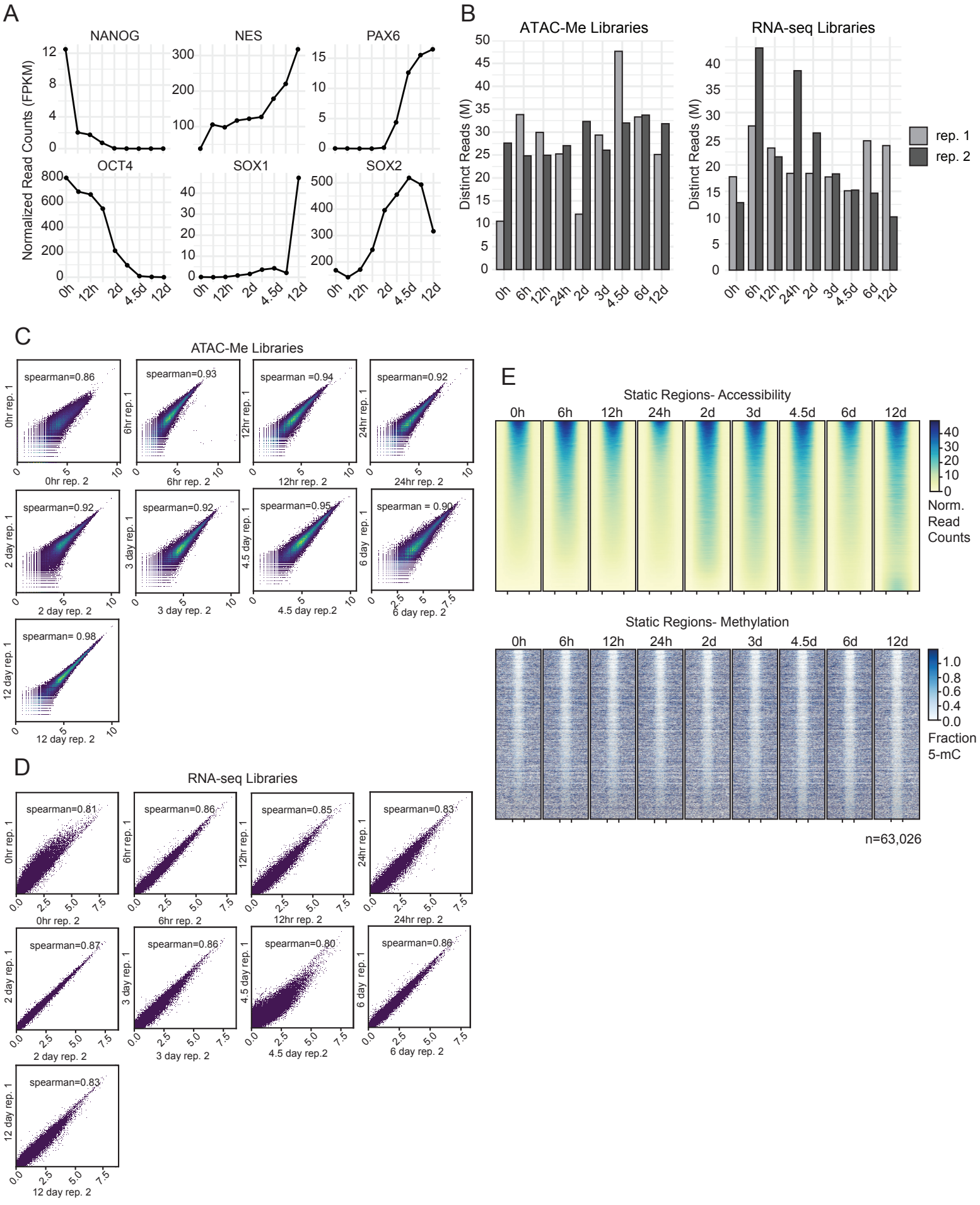
A
NANOG
NES
PAX6
OCT4
SOX1
SOX2
Normalized Read Counts (FPKM)
0h
12h
2d
4.5d
12d
B
ATAC-Me Libraries
RNA-seq Libraries
Distinct Reads (M)
0h
6h
12h
24h
2d
3d
4.5d
6d
12d
rep. 1
rep. 2
C
ATAC-Me Libraries
spearman=0.86
spearman=0.93
spearman =0.94
spearman=0.92
spearman=0.92
spearman=0.92
spearman=0.95
spearman = 0.90
spearman= 0.98
0hr rep. 1
6hr rep. 1
12hr rep. 1
24hr rep. 1
2 day rep. 1
3 day rep. 1
4.5 day rep. 1
6 day rep. 1
12 day rep. 1
0hr rep. 2
6hr rep. 2
12hr rep. 2
24hr rep. 2
2 day rep. 2
3 day rep. 2
4.5 day rep.2
6 day rep. 2
12 day rep. 2
D
RNA-seq Libraries
spearman=0.81
spearman=0.86
spearman=0.85
spearman=0.83
spearman=0.87
spearman=0.86
spearman=0.80
spearman=0.86
spearman=0.83
E
Static Regions- Accessibility
Norm. Read Counts
Static Regions- Methylation
Fraction 5-mC
n=63,026

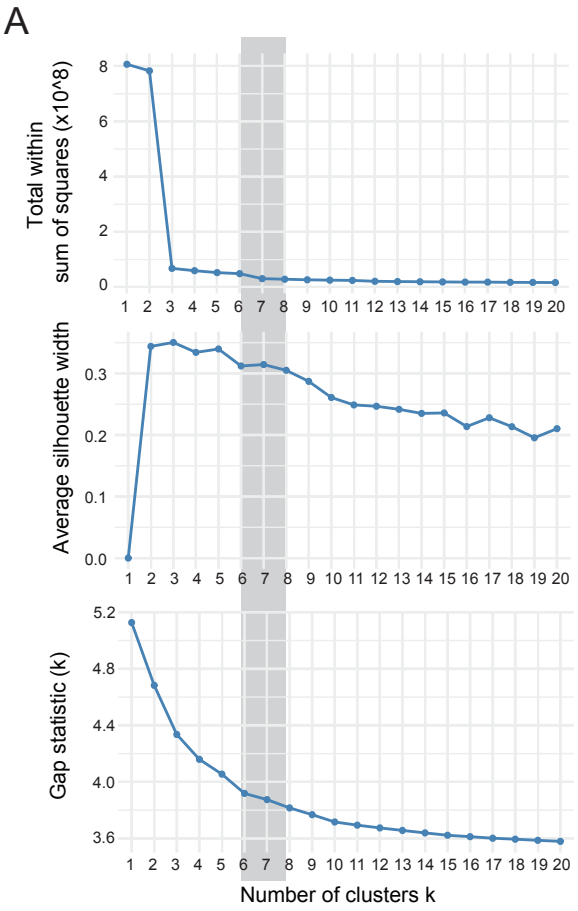
A
Total within sum of squares (x10^8)
Average silhouette width
Gap statistic (k)
Number of clusters k

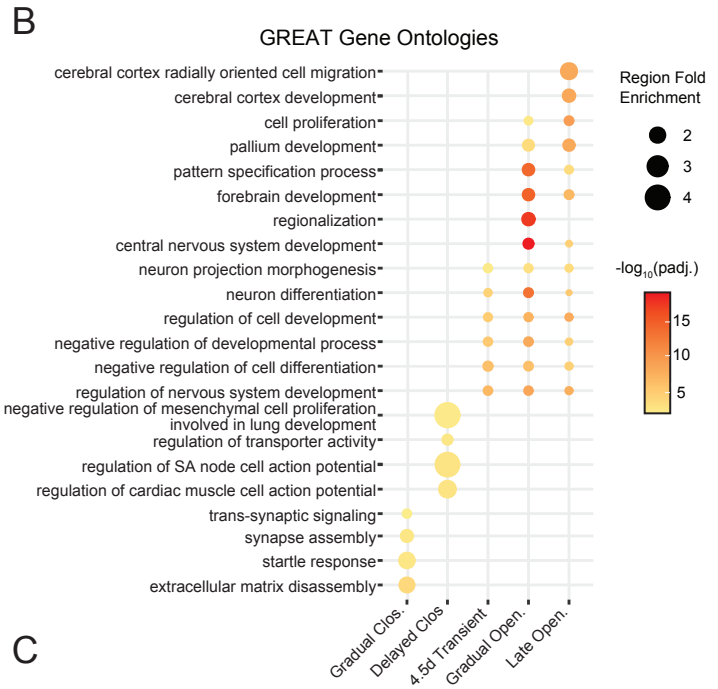
B
GREAT Gene Ontologies
cerebral cortex radially oriented cell migration
cerebral cortex development
cell proliferation
pallium development
pattern specification process
forebrain development
regionalization
central nervous system development
neuron projection morphogenesis
neuron differentiation
regulation of cell development
negative regulation of developmental process
negative regulation of cell differentiation
regulation of nervous system development
negative regulation of mesenchymal cell proliferation involved in lung development
regulation of transporter activity
regulation of SA node cell action potential
regulation of cardiac muscle cell action potential
trans-synaptic signaling
synapse assembly
startle response
extracellular matrix disassembly
Gradual Clos.
Delayed Clos
4.5d Transient
Gradual Open.
Late Open.
Region Fold Enrichment
-log10(padj.)

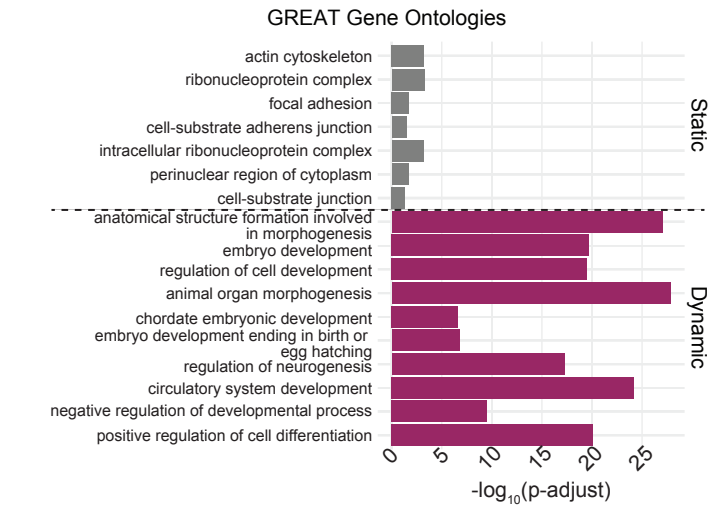
C
GREAT Gene Ontologies
actin cytoskeleton
ribonucleoprotein complex
focal adhesion
cell-substrate adherens junction
intracellular ribonucleoprotein complex
perinuclear region of cytoplasm
cell-substrate junction
anatomical structure formation involved in morphogenesis
embryo development
regulation of cell development
animal organ morphogenesis
chordate embryonic development
embryo development ending in birth or egg hatching
regulation of neurogenesis
circulatory system development
negative regulation of developmental process
positive regulation of cell differentiation
Static
Dynamic
-log10(p-adjust)

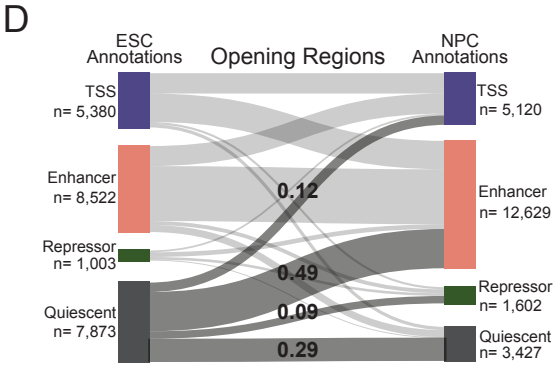
D
ESC Annotations
Opening Regions
NPC Annotations
TSS n= 5,380
Enhancer n= 8,522
Repressor n= 1,003
Quiescent n= 7,873
TSS n= 5,120
Enhancer n= 12,629
Repressor n= 1,602
Quiescent n= 3,427
0.12
0.49
0.09
0.29

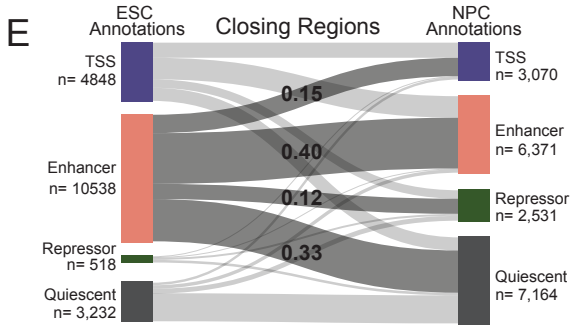
E
ESC Annotations
Closing Regions
NPC Annotations
TSS n= 4848
Enhancer n= 10538
Repressor n= 518
Quiescent n= 3,232
TSS n= 3,070
Enhancer n= 6,371
Repressor n= 2,531
Quiescent n= 7,164
0.15
0.40
0.12
0.33

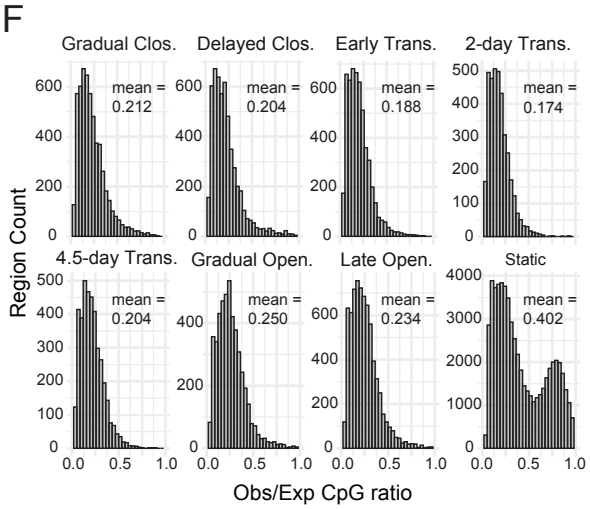
F
Gradual Clos.
Delayed Clos.
Early Trans.
2-day Trans.
4.5-day Trans.
Gradual Open.
Late Open.
Static
mean = 0.212
mean = 0.204
mean = 0.188
mean = 0.174
mean = 0.204
mean = 0.250
mean = 0.234
mean = 0.402
Region Count
Obs/Exp CpG ratio

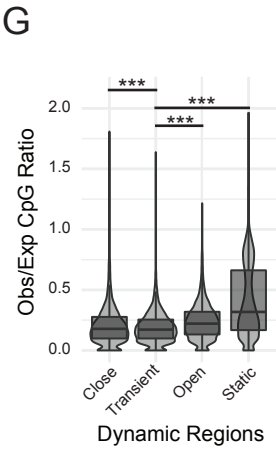
G
Obs/Exp CpG Ratio
***
***
***
Close
Transient
Open
Static
Dynamic Regions

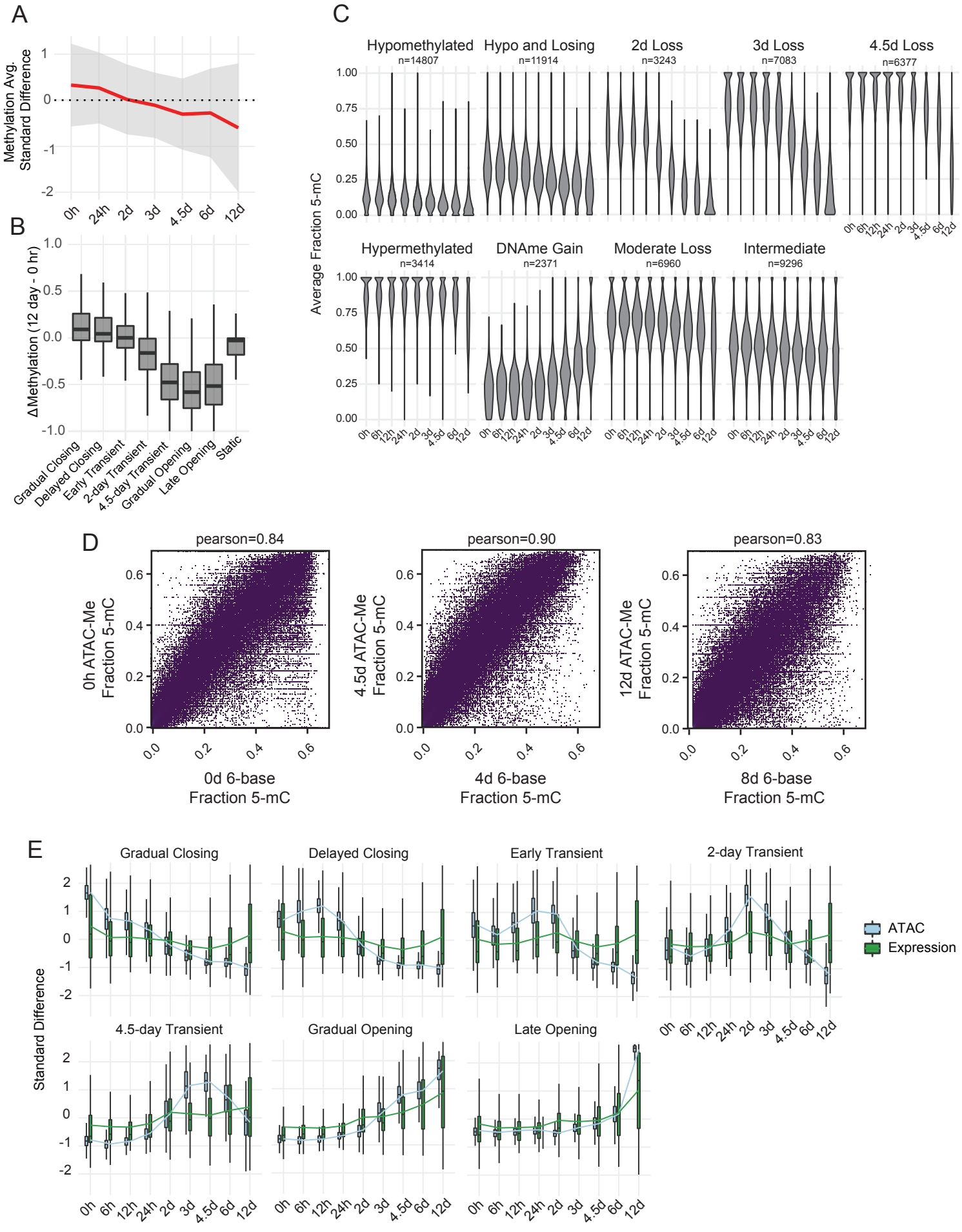
A
Methylation Avg. Standard Difference
1
0
-1
-2
0h
24h
2d
3d
4.5d
6d
12d
B
ΔMethylation (12 day - 0 hr)
1.0
0.5
0.0
-0.5
-1.0
Gradual Closing
Delayed Closing
Early Transient
2-day Transient
4.5-day Transient
Gradual Opening
Late Opening
Static
C
Hypomethylated
n=14807
Hypo and Losing
n=11914
2d Loss
n=3243
3d Loss
n=7083
4.5d Loss
n=6377
Hypermethylated
n=3414
DNAme Gain
n=2371
Moderate Loss
n=6960
Intermediate
n=9296
Average Fraction 5-mC
1.00
0.75
0.50
0.25
0.00
0h
6h
12h
24h
2d
3d
4.5d
6d
12d
D
pearson=0.84
pearson=0.90
pearson=0.83
0h ATAC-Me Fraction 5-mC
4.5d ATAC-Me Fraction 5-mC
12d ATAC-Me Fraction 5-mC
0.6
0.4
0.2
0.0
0d 6-base Fraction 5-mC
4d 6-base Fraction 5-mC
8d 6-base Fraction 5-mC
E
Gradual Closing
Delayed Closing
Early Transient
2-day Transient
4.5-day Transient
Gradual Opening
Late Opening
Standard Difference
2
1
0
-1
-2
ATAC
Expression

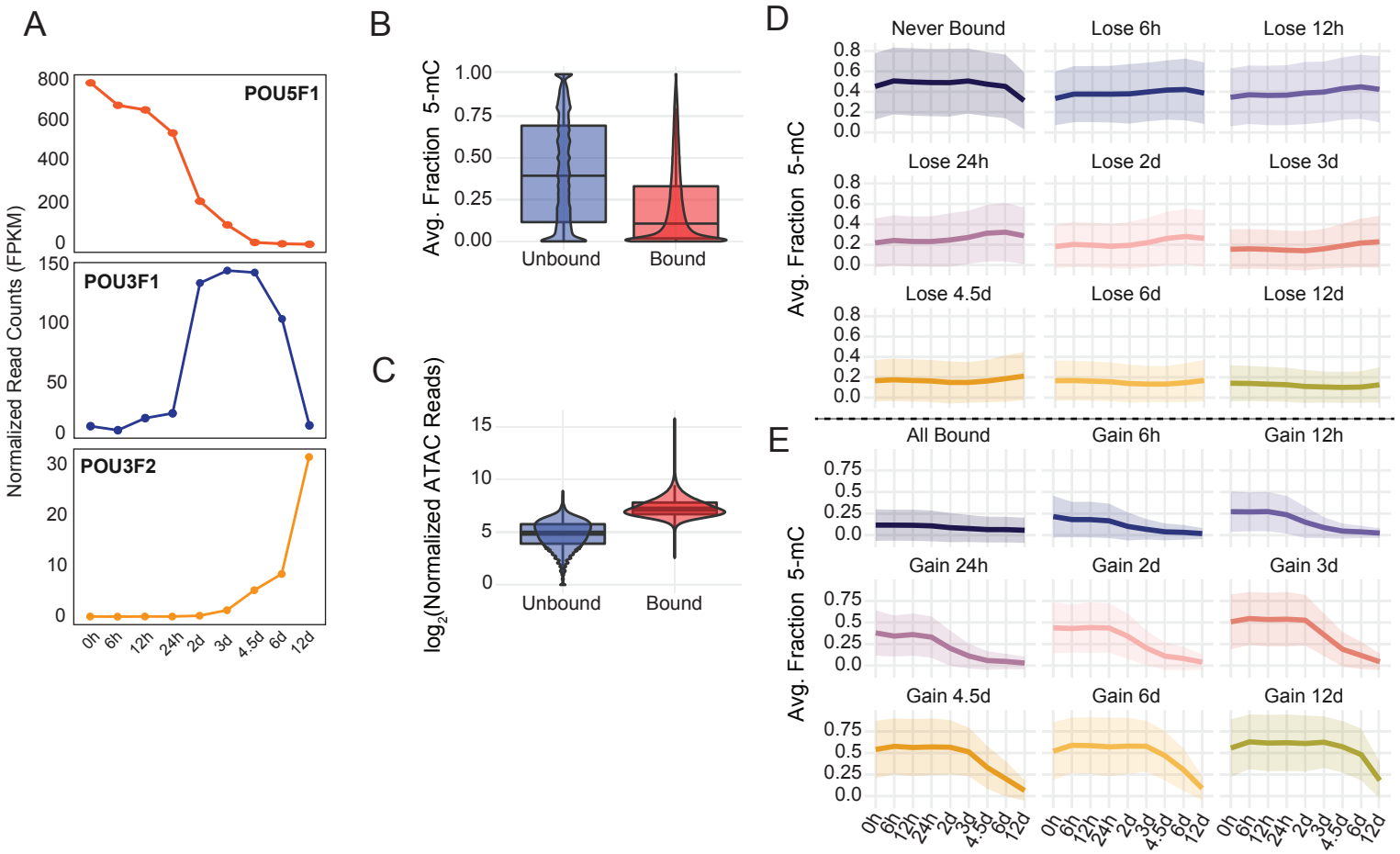
A
POU5F1
POU3F1
POU3F2
Normalized Read Counts (FPKM)
0h
6h
12h
24h
2d
3d
4.5d
6d
12d
B
Avg. Fraction 5-mC
Unbound
Bound
C
log2(Normalized ATAC Reads)
Unbound
Bound
D
Never Bound
Lose 6h
Lose 12h
Lose 24h
Lose 2d
Lose 3d
Lose 4.5d
Lose 6d
Lose 12d
Avg. Fraction 5-mC
E
All Bound
Gain 6h
Gain 12h
Gain 24h
Gain 2d
Gain 3d
Gain 4.5d
Gain 6d
Gain 12d
Avg. Fraction 5-mC

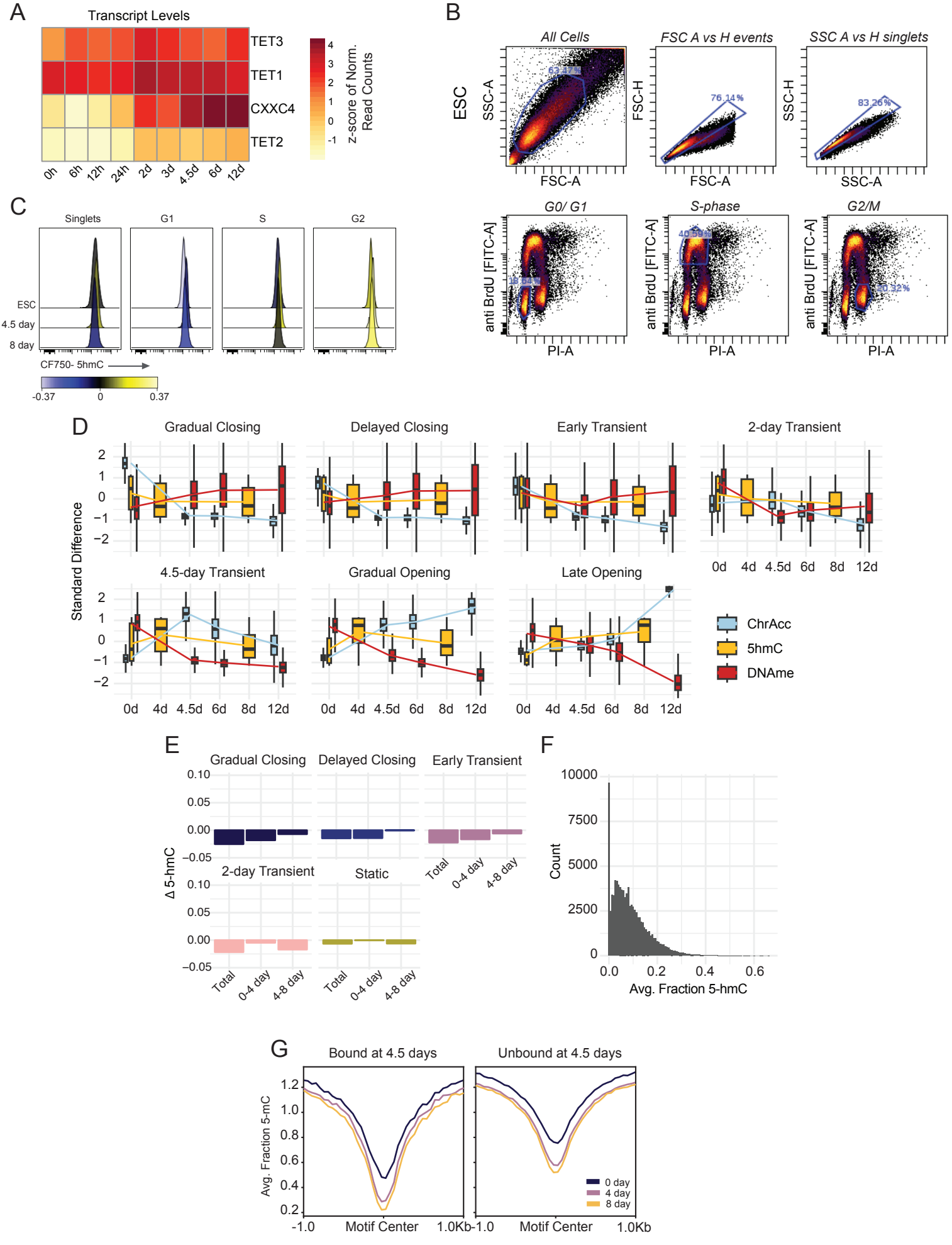
A
Transcript Levels
TET3
TET1
CXXC4
TET2
0h
6h
12h
24h
2d
3d
4.5d
6d
12d
z-score of Norm. Read Counts
B
ESC
All Cells
FSC A vs H events
SSC A vs H singlets
SSC-A
FSC-A
FSC-H
SSC-H
63.17%
76.14%
83.26%
G0/ G1
S-phase
G2/M
anti BrdU [FITC-A]
PI-A
C
Singlets
G1
S
G2
ESC
4.5 day
8 day
CF750- 5hmC
-0.37
0
0.37
D
Gradual Closing
Delayed Closing
Early Transient
2-day Transient
4.5-day Transient
Gradual Opening
Late Opening
Standard Difference
0d
4d
4.5d
6d
8d
12d
ChrAcc
5hmC
DNAme
E
Gradual Closing
Delayed Closing
Early Transient
2-day Transient
Static
Δ 5-hmC
Total
0-4 day
4-8 day
F
Count
Avg. Fraction 5-hmC
G
Bound at 4.5 days
Unbound at 4.5 days
Avg. Fraction 5-mC
Motif Center
0 day
4 day
8 day

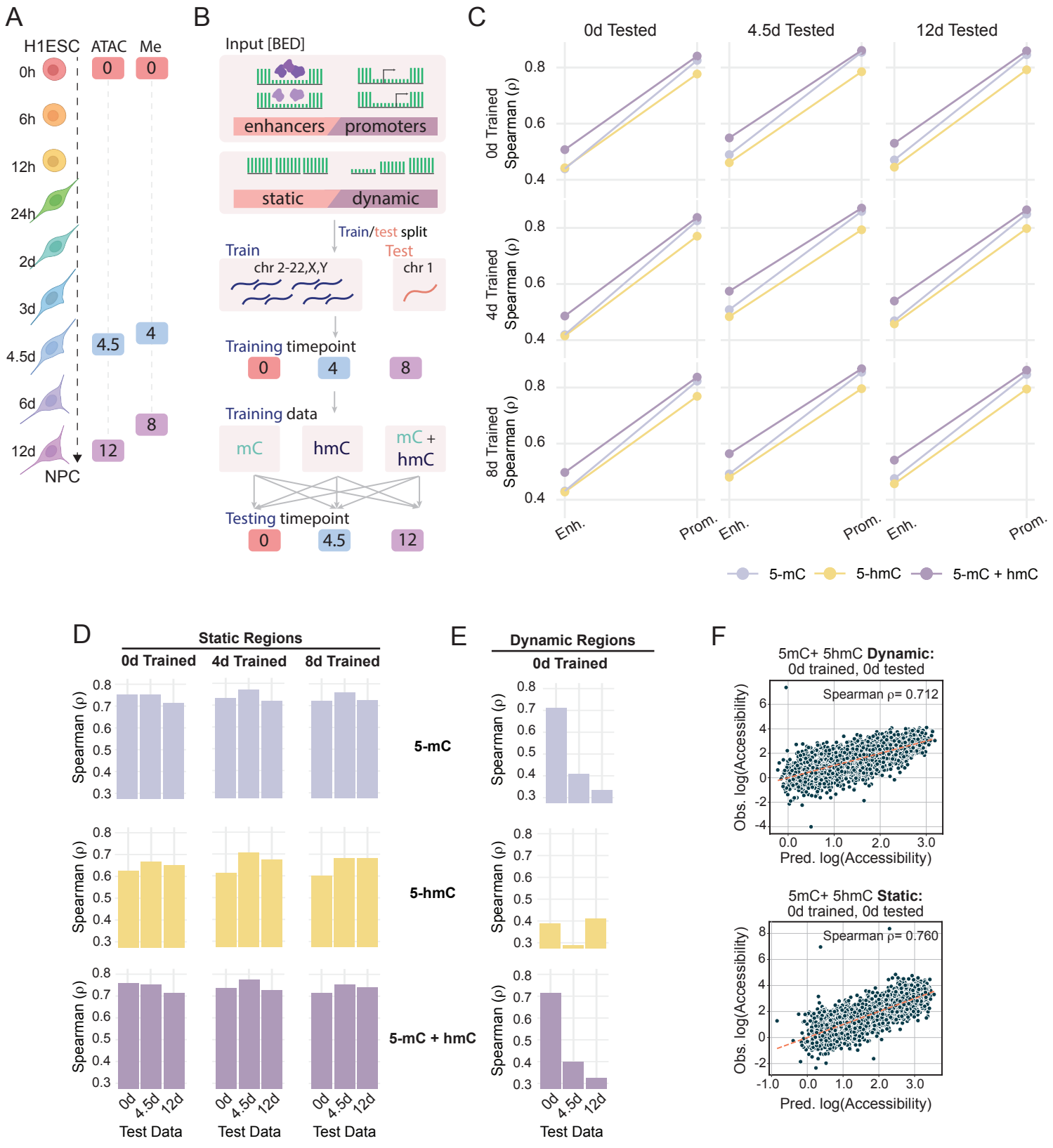
A
H1ESC
ATAC
Me
0h
6h
12h
24h
2d
3d
4.5d
6d
12d
NPC
0
0
4.5
4
8
12
B
Input [BED]
enhancers
promoters
static
dynamic
Train/test split
Train
Test
chr 2-22,X,Y
chr 1
Training timepoint
0
4
8
Training data
mC
hmC
mC + hmC
Testing timepoint
0
4.5
12
C
0d Tested
4.5d Tested
12d Tested
0d Trained Spearman (ρ)
4d Trained Spearman (ρ)
8d Trained Spearman (ρ)
Enh.
Prom.
5-mC
5-hmC
5-mC + hmC
D
Static Regions
0d Trained
4d Trained
8d Trained
Spearman (ρ)
5-mC
5-hmC
5-mC + hmC
Test Data
E
Dynamic Regions
0d Trained
F
5mC+ 5hmC Dynamic:
0d trained, 0d tested
Spearman ρ= 0.712
Obs. log(Accessibility)
Pred. log(Accessibility)
5mC+ 5hmC Static:
0d trained, 0d tested
Spearman ρ= 0.760

Table S1: Library, sequencing, and analysis statistics for each ATAC-Me sample.

ATAC-Me Sequencing				
Sample	Final library concentration (ng/ul)	Total reads	CpGs (coverage ≥ 5X)	Peak number
0hr A	5.93	67213113	1302926	46961
0hr B	1.09	58626341	2089056	
6hr A	6.88	103292803	2981980	46915
6hr B	16	60019065	2036771	
12hr A	11.1	88052404	2650643	42019
12hr B	5.88	68990381	1732449	
24hr A	6.86	68152510	2124207	27765
24hr B	5.32	69078947	1869887	
48hr A	1.05	177315084	2079575	65270
48hr B	8.28	79665573	2696196	
72hr A	15.3	90632062	3478202	57044
72hr B	2.71	71355801	2347331	
4.5day A	2.23	105550194	4217114	58888
4.5day B	8.16	72500021	2769749	
6day A	4.36	55513844	2995283	33418
6day B	9.65	60194982	2684612	
12day A	13.4	55598687	2067362	59581
12day B	8.54	75398649	2456311	

Table S2: Library, sequencing, and analysis statistics for each RNA-seq sample.

RNA sequencing				
Sample	Final library concentration (ng/ul)	Input reads	Uniquely mapped reads	Filtered reads
0hr A	27.8	31909040	22158598	8610268
0hr B	20.3	27715446	18288951	6593643
6hr A	0.684	49931050	35668744	13271468
6hr B	5.27	16216974	12303359	20646873
12hr A	22	43495053	29803224	11368648
12hr B	19.1	23324620	17976459	10318180
24hr A	15.3	32461243	23247257	8797646
24hr B	24.9	25032726	18718534	17894918
48hr A	17.1	30598220	22546414	8750219
48hr B	17.5	44161371	32901592	12379472
72hr A	6.66	34465624	22359612	8632510
72hr B	30.9	31959301	22174802	8709773
4.5day A	7.25	31953740	19735284	8013688
4.5day B	20.3	63603786	48041193	7378077
6day A	4.38	49554234	32078907	12392128
6day B	15.8	36253322	27096703	7138882
12day A	17.8	41643300	28975427	11522785
12day B	12.7	76323733	57066247	4910512

Table S3: Full list of TF motifs enriched in each cluster, as visualized in Figure 2D.

log_pval	percentFold	Motif	Cluster
-2031	9.99126638	OCT4-SOX2-TCF-NANOG	Delayed Closing
-1111	3.9653092	OCT4	Delayed Closing
-927.5	3.98214286	OCT6	Delayed Closing
-879.1	4.59305211	Brn1	Delayed Closing
-834.8	4.89675516	Jun-AP1	Delayed Closing
-812.1	4.10042735	Fosl2	Delayed Closing
-804.8	3.43647235	Fra2	Delayed Closing
-767.4	3.15374677	Fra1	Delayed Closing
-695	2.76012461	Atf3	Delayed Closing
-688.9	2.98867925	JunB	Delayed Closing
-656.4	2.73113709	BATF	Delayed Closing
-651.4	3.95853659	OCT11	Delayed Closing
-630.4	2.52126697	AP-1	Delayed Closing
-545.1	3.67901235	OCT2	Delayed Closing
-458.6	5.52631579	CTCF	Delayed Closing
-456.6	4.01403509	Bach2	Delayed Closing
-376.4	3.82758621	BORIS	Delayed Closing
-322.9	1.58471633	Sox3	Delayed Closing
-319	2.01482127	Zic3	Delayed Closing
-316.5	1.7875895	TEAD1	Delayed Closing
-312.3	1.84667115	TEAD4	Delayed Closing
-290.1	1.95287061	TEAD	Delayed Closing
-277.3	1.66961959	TEAD3	Delayed Closing
-264.9	1.7847841	Zic	Delayed Closing
-257.9	2.01147028	TEAD2	Delayed Closing
-1695	10.8218391	OCT4-SOX2-TCF-NANOG	Early Transient
-911.5	2.64480472	Zic3	Early Transient
-742.9	1.9586743	Sox3	Early Transient
-716.2	3.64391144	OCT4	Early Transient
-710.7	2.4132948	Unknown-ESC-element	Early Transient
-679.2	2.23247232	Zic	Early Transient
-651.3	3.79431072	OCT6	Early Transient
-624.2	4.40123457	Brn1	Early Transient
-590	1.87987988	Sox10	Early Transient
-538.4	2.31458843	Sox2	Early Transient
-454.4	1.808491	Sox6	Early Transient
-451.5	3.70381232	OCT11	Early Transient

-389.6	2.07322835	Sox4	Early Transient
-366.9	2.22312373	Sox17	Early Transient
-348.8	3.39318885	OCT2	Early Transient
-316.1	1.80680437	Sox15	Early Transient
-225	2.83692308	BORIS	Early Transient
-214.6	2.69774011	Zfp281	Early Transient
-197.8	1.70188133	Sox9	Early Transient
-192.7	1.52030217	Tcf12	Early Transient
-182.1	3.26455026	CTCF	Early Transient
-174.3	2.456	Foxa3	Early Transient
-151.9	1.74374374	Foxa2	Early Transient
-150.5	1.31877729	Ascl1	Early Transient
-148.1	1.40143369	Ap4	Early Transient
-1246	9.49350649	OCT4-SOX2-TCF-NANOG	Gradual Closing
-835.9	7.66	CTCF	Gradual Closing
-738.6	5.10181818	BORIS	Gradual Closing
-639.4	3.7826087	OCT6	Gradual Closing
-637.8	3.5502008	OCT4	Gradual Closing
-598.8	4.31309904	Brn1	Gradual Closing
-586.4	2.17296223	TEAD1	Gradual Closing
-497	1.9774044	TEAD3	Gradual Closing
-478.2	2.10192445	TEAD4	Gradual Closing
-461.3	1.78619756	Sox3	Gradual Closing
-443.2	2.2731569	TEAD	Gradual Closing
-420.6	3.68488746	OCT11	Gradual Closing
-410.3	2.33953998	TEAD2	Gradual Closing
-349.1	1.79490085	Sp5	Gradual Closing
-336.2	3.4	OCT2	Gradual Closing
-316.1	1.81242079	Fli1	Gradual Closing
-309	1.56860465	ERG	Gradual Closing
-294.5	1.8239726	Etv2	Gradual Closing
-280.2	2.00486855	EWS:ERG-fusion	Gradual Closing
-278.3	1.61842105	ETV1	Gradual Closing
-276.9	1.62214829	Sox10	Gradual Closing
-274.8	1.74937186	ETS1	Gradual Closing
-266.6	2.02628812	KLF3	Gradual Closing
-263.7	2.11678832	EWS:FLI1-fusion	Gradual Closing
-261.7	1.6971831	ETV4	Gradual Closing
-1269	2.33985765	Sox3	4.5-day Transient

-1102	2.30503381	Sox10	4.5-day Transient
-1080	3.10671378	Sox2	4.5-day Transient
-877.9	2.21721802	Sox6	4.5-day Transient
-844.8	2.82122905	Sox4	4.5-day Transient
-794	2.42909664	Sox15	4.5-day Transient
-762.1	3.0596745	Sox17	4.5-day Transient
-570.8	2.39738562	Otx2	4.5-day Transient
-488.3	2.27561608	Lhx2	4.5-day Transient
-486.9	2.29081295	Sox9	4.5-day Transient
-434.2	1.85359902	Lhx3	4.5-day Transient
-412.9	2.10409146	Lhx1	4.5-day Transient
-357.8	1.84932777	LXH9	4.5-day Transient
-347.8	2.48915401	Dlx3	4.5-day Transient
-306.4	1.50849744	Nkx6.1	4.5-day Transient
-246.2	1.93366619	Zic3	4.5-day Transient
-242.5	1.52179487	Isl1	4.5-day Transient
-239.8	1.67870201	Tcf12	4.5-day Transient
-230	1.57984791	Ap4	4.5-day Transient
-230	1.67941454	Tcf21	4.5-day Transient
-225.2	1.8777079	Unknown-ESC-element	4.5-day Transient
-219.9	1.76703553	Zic	4.5-day Transient
-188.7	1.76801058	Myf5	4.5-day Transient
-185.5	1.71317365	MyoD	4.5-day Transient
-172.2	1.91316527	LEF1	4.5-day Transient
-1439	1.89492326	Sox3	Late Opening
-1356	1.92666667	Sox10	Late Opening
-1102	2.30439684	Sox2	Late Opening
-905	1.74181478	Sox6	Late Opening
-796.8	2.15160703	Sox9	Late Opening
-788.6	1.89222842	Sox15	Late Opening
-783.7	2.25069252	Sox17	Late Opening
-775.4	2.11406619	Sox4	Late Opening
-761.4	1.95871782	TEAD1	Late Opening
-728.1	1.84589331	TEAD3	Late Opening
-678.1	1.9977591	TEAD4	Late Opening
-630	6.60169492	Rfx2	Late Opening
-594	7.1122449	RFX	Late Opening
-582.8	2.0208605	TEAD	Late Opening
-546.4	1.76744186	Lhx2	Late Opening

-481.2	1.58559499	LXH9	Late Opening
-473.3	4.68823529	X-box	Late Opening
-431.6	3.25739645	Rfx1	Late Opening
-421.8	1.62823726	Lhx1	Late Opening
-401	1.98982188	TEAD2	Late Opening
-398.8	1.4632785	Lhx3	Late Opening
-366.2	1.31169094	Nkx6.1	Late Opening
-327.6	2.40142096	Rfx5	Late Opening
-301.3	1.37398594	Isl1	Late Opening
-259	3.76351351	PAX6	Late Opening
-748.5	2.09595202	Sox3	2-day Transient
-668.1	2.68493151	Zic3	2-day Transient
-642.8	2.70476911	Sox2	2-day Transient
-631.6	2.4407497	Zic	2-day Transient
-612.8	2.02962085	Sox10	2-day Transient
-576.8	2.51818182	Unknown-ESC-element	2-day Transient
-547.1	2.03432003	Sox6	2-day Transient
-456.9	2.65259117	Sox17	2-day Transient
-455.6	2.15005663	Sox15	2-day Transient
-445.1	2.36457565	Sox4	2-day Transient
-288.7	2.01215395	Sox9	2-day Transient
-247.1	1.94718555	Otx2	2-day Transient
-199.6	3.98429319	OCT4-SOX2-TCF-NANOG	2-day Transient
-140.5	1.53445851	Tcf12	2-day Transient
-137.7	2.60773481	Brn1	2-day Transient
-136.3	1.46016323	Ap4	2-day Transient
-127.3	2.15017065	OCT4	2-day Transient
-124.9	1.51735941	Tcf21	2-day Transient
-124.7	1.14525678	SCL	2-day Transient
-123.6	1.81681682	LEF1	2-day Transient
-106.4	1.44613321	Lhx3	2-day Transient
-102.8	2.10331384	OCT6	2-day Transient
-94.25	1.51461632	MyoD	2-day Transient
-91.34	1.56290439	Lhx2	2-day Transient
-91.21	1.54371585	Myf5	2-day Transient
-1413	2.17396866	Sox3	Gradual Opening
-1243	2.89943074	Sox2	Gradual Opening
-1148	2.11062246	Sox10	Gradual Opening
-905.3	2.01762425	Sox6	Gradual Opening

-884.6	2.56257822	Sox4	Gradual Opening
-824.8	2.2156587	Sox15	Gradual Opening
-759.2	2.68421053	Sox17	Gradual Opening
-580	2.19725864	Sox9	Gradual Opening
-526.8	2.0541555	Lhx2	Gradual Opening
-480.6	1.72080166	Lhx3	Gradual Opening
-472.3	1.94969819	Lhx1	Gradual Opening
-420.6	1.74890916	LXH9	Gradual Opening
-342.9	2.1630149	Dlx3	Gradual Opening
-342.2	1.43294839	Nkx6.1	Gradual Opening
-331	1.88116459	Otx2	Gradual Opening
-298.9	5	Rfx2	Gradual Opening
-289.3	5.32786885	RFX	Gradual Opening
-269.8	4.58823529	PAX6	Gradual Opening
-263	1.46126761	Isl1	Gradual Opening
-196.8	3.68539326	X-box	Gradual Opening
-144.9	1.40449853	Ap4	Gradual Opening
-140.2	2.38258575	Rfx1	Gradual Opening
-130.1	1.65622424	LEF1	Gradual Opening
-99.23	1.44748858	MyoD	Gradual Opening
-99.14	1.38705234	Tcf21	Gradual Opening

Table S4: Full list of TF displaying differential expression during the time course clustered by expression pattern, as visualized in Figure 4C**.**

Transcription Factor	Cluster number
ZNF684	1
MIER1	1
LHX8	1
NHLH2	1
NR5A2	1
TFB2M	1
ZNF124	1
CEBPZ	1
BOLA3	1
KCMF1	1
LRRFIP1	1
ZNF860	1
ZNF35	1
HLTF	1
SKIL	1
ZNF876P	1
LYAR	1
NFXL1	1

ZFP42	1
NR3C1	1
ZNF165	1
POU5F1	1
ZBTB24	1
HEY2	1
NCOA7	1
ETV1	1
NFE2L3	1
DNAJC2	1
ZNF398	1
ZMAT4	1
THAP1	1
TCF24	1
PRDM14	1
MSC	1
TERF1	1
HNF4G	1
RUNX1T1	1
POU5F1B	1
ZNF483	1
MKX	1
ZNF239	1
ZNF485	1
TFAM	1
NOC3L	1
PCGF6	1
VENTX	1
ZNF195	1
ESRRA	1
ETS1	1
ZBTB44	1
NANOG	1
BHLHE41	1
ARNTL2	1
ATF1	1
YEATS4	1
PAWR	1
GTF3A	1
FOXN3	1
ZNF770	1
ONECUT1	1
ZNF267	1
SNAI3	1
ZNF232	1
PHB	1
SMAD7	1
ZNF57	1
ZNF121	1

ZNF878	1
ZNF90	1
ZNF146	1
ZNF114	1
ZNF649	1
ZNF836	1
ZNF28	1
ZNF468	1
ZNF845	1
ZNF761	1
ZNF813	1
TCF15	1
OVOL2	1
PHF5A	1
ZNF670	2
MYT1L	2
ATF2	2
ZNF385D	2
ETV5	2
LCORL	2
RBPJ	2
CLOCK	2
ZNF354A	2
ZNF184	2
RUNX2	2
ZUFSP	2
SNAI2	2
RORB	2
ZBTB6	2
ZNF143	2
THAP2	2
ZNF605	2
ZFP1	2
IRF8	2
ZNF624	2
KAT7	2
ZNF555	2
ZNF566	2
ZNF225	2
ZNF234	2
ZNF615	2
ZNF415	2
ZNF765	2
ID1	2
TP73	3
ENO1	3
ID3	3
GRHL3	3
ZNF593	3

ZC3H12A	3
FOXE3	3
FOXD3	3
TTF2	3
ZNF697	3
ZBTB7B	3
ZNF281	3
ELF3	3
IRF6	3
ATF3	3
BATF3	3
MYCN	3
PREB	3
EPAS1	3
BCL11A	3
EMX1	3
TCF7L1	3
FOXI3	3
TFCP2L1	3
NFE2L2	3
SP110	3
SP140	3
GBX2	3
HES6	3
THAP4	3
BHLHE40	3
CSRNP1	3
NFKBIZ	3
FOXL2	3
AHRR	3
IRX4	3
ZNF622	3
IRF1	3
MXD3	3
IRF4	3
JARID2	3
ZFP57	3
TCF19	3
HMGA1	3
TFEB	3
NFKBIE	3
ZBTB2	3
MAFK	3
AHR	3
PARP12	3
NKX3-1	3
CEBPD	3
GRHL2	3
TRPS1	3

ZHX2	3
MYC	3
MAFA	3
SMARCA2	3
NFIB	3
BNC2	3
NFX1	3
PAX5	3
LHX6	3
ZNF488	3
NFKB2	3
NKX1-2	3
FOXI2	3
UTF1	3
ARNTL	3
E2F8	3
ZBTB3	3
OVOL1	3
FOSL1	3
PGR	3
ZNF202	3
TEAD4	3
PHB2	3
YBX3	3
VDR	3
POU6F1	3
DDIT3	3
NOC4L	3
PSPC1	3
FOXO1	3
TFDP1	3
JDP2	3
ZBTB42	3
BNC1	3
ZSCAN2	3
MESP2	3
ZSCAN10	3
ZNF469	3
TAX1BP3	3
YBX2	3
SOX15	3
MLX	3
ETV4	3
UBTF	3
SP6	3
NFE2L1	3
SMARCD2	3
FOXJ1	3
MAFG	3

TGIF1	3
KLF16	3
NR2F6	3
ZNF101	3
TSHZ3	3
DPF1	3
NFKBIB	3
ZNF296	3
FOXA3	3
IRF3	3
ATF5	3
SPIB	3
ZNF134	3
ZNF552	3
FOXA2	3
DNMT3B	3
E2F1	3
MYBL2	3
CEBPB	3
ZFP64	3
OLIG2	3
OLIG1	3
ERG	3
XBP1	3
MAFF	3
ATF4	3
TFE3	3
POU3F4	3
ELF4	3
MYCL	4
DMBX1	4
ETV3L	4
PBX1	4
RXRG	4
PRRX1	4
MTA3	4
SP5	4
THRB	4
ZBTB47	4
HESX1	4
MYB	4
OLIG3	4
CREB3L2	4
ASH2L	4
TOX	4
FOXH1	4
FOXB2	4
LMX1B	4
BARHL1	4

HHEX	4
PAX2	4
HMX3	4
HMX2	4
CREB3L1	4
BATF2	4
PHOX2A	4
POU2F3	4
PKNOX2	4
RARG	4
NFE2	4
STAT6	4
GLI1	4
ZIC5	4
ZIC2	4
NKX2-8	4
DPF3	4
CEBPA	4
CRX	4
SNAI1	4
TFAP2C	4
CTCFL	4
PCBP3	4
FOXO4	4
MBNL3	4
ZIC3	4
HES3	5
ZBTB17	5
ZNF436	5
E2F2	5
ZNF362	5
ZSCAN20	5
POU3F1	5
FOXO6	5
ZCCHC11	5
ALX3	5
PHTF1	5
GABPB2	5
RFX5	5
GATAD2B	5
ASH1L	5
IFI16	5
LMX1A	5
TBX19	5
ZBTB41	5
LHX9	5
ZC3H11A	5
ELK4	5
RCOR3	5

SOX11	5
ID2	5
ZNF512	5
SIX3	5
REL	5
OTX1	5
ZNF514	5
ZC3H8	5
ZC3H6	5
ZEB2	5
MBD5	5
CSRNP3	5
SP9	5
ZNF385B	5
ZNF804A	5
SATB1	5
NR1D2	5
ZNF445	5
PCBP4	5
ZNF148	5
TFDP2	5
MECOM	5
SOX2	5
BCL6	5
HES1	5
MXD4	5
ZNF518B	5
HOPX	5
REST	5
NKX6-1	5
TET2	5
NEUROG2	5
IRX1	5
ZNF608	5
ZFP2	5
ZNF879	5
FOXC1	5
SOX4	5
ZSCAN9	5
ZSCAN26	5
ZKSCAN3	5
ZSCAN23	5
PBX2	5
ZBTB22	5
ZNF451	5
ZNF292	5
HSF2	5
MLLT4	5
ZNF853	5

POU6F2	5
ZNF713	5
ZNF117	5
ZNF789	5
ZKSCAN1	5
CUX1	5
KMT2E	5
HBP1	5
FEZF1	5
ZNF467	5
SMARCD3	5
KMT2C	5
ZNF395	5
HMBOX1	5
PURG	5
PLAG1	5
ZFHX4	5
ZBTB10	5
GLI4	5
ZNF517	5
ZNF250	5
RFX3	5
MLLT3	5
ZFP37	5
ZBTB26	5
NR5A1	5
NR6A1	5
PBX3	5
PRRX2	5
ZNF438	5
ZNF248	5
ZNF25	5
MXI1	5
ASCL2	5
ZNF214	5
TUB	5
DBX1	5
KMT2A	5
SOX5	5
ZNF641	5
ZNF740	5
SP7	5
ZC3H10	5
SMARCC2	5
STAT2	5
NR2C1	5
LHX5	5
ZNF664	5
ZNF84	5

TSC22D1	5
DACH1	5
SOX21	5
ZNF219	5
HOMEZ	5
NFATC4	5
FOXA1	5
OTX2	5
ARID4A	5
SIX6	5
VSX2	5
FOS	5
ESRRB	5
GSC	5
ZNF280D	5
FOXB1	5
SMAD6	5
SCAPER	5
ZNF710	5
ZNF785	5
TOX3	5
IRX3	5
IRX5	5
ZFP90	5
ZNF19	5
MAF	5
ZBTB4	5
ZNF287	5
MLLT6	5
THRA	5
ZNF385C	5
STAT5B	5
EZH1	5
DLX3	5
VEZF1	5
ZNF519	5
ZNF521	5
SETBP1	5
SMAD2	5
ZBTB7C	5
TCF4	5
RAX	5
ZNF516	5
SALL3	5
ZNF558	5
ZNF699	5
ZNF559-ZNF177	5
ZNF177	5
ZNF266	5

ZNF846	5
ZNF653	5
ZNF441	5
ZNF491	5
ZNF440	5
ZNF439	5
ZNF69	5
ZNF763	5
ZNF433	5
ZNF709	5
JUND	5
PBX4	5
ZNF737	5
ZNF91	5
ZFP14	5
ZNF529	5
ZNF568	5
ZNF585A	5
HKR1	5
ZNF793	5
ZNF571	5
ZFP30	5
ZNF781	5
ZNF546	5
ZNF780B	5
ZNF428	5
ZNF155	5
ZNF224	5
ZNF226	5
ZNF112	5
ZNF285	5
SIX5	5
ZNF432	5
ZNF610	5
ZNF880	5
ZNF83	5
ZNF611	5
ZNF702P	5
ZNF579	5
ZNF580	5
ZNF419	5
ZNF211	5
ZNF606	5
ZNF135	5
ZSCAN18	5
ZNF329	5
ZNF446	5
MZF1	5
ZNF343	5

C20orf194	5
BMP2	5
TGIF2	5
ZHX3	5
ZNF334	5
NCOA3	5
SALL4	5
MYT1	5
ZNF280A	5
ZNF70	5
SOX10	5
TEF	5
KLF8	5
ATRX	5
ZNF711	5
SMARCA1	5
ZNF449	5
HES4	6
HES5	6
PRDM16	6
CASZ1	6
HEYL	6
HIVEP3	6
DMRTA2	6
JUN	6
NHLH1	6
MAEL	6
ZBTB37	6
PROX1	6
ESRRG	6
ZBTB18	6
FOSL2	6
MEIS1	6
MXD1	6
VAX2	6
ATOH8	6
AFF3	6
POU3F3	6
IKZF2	6
EOMES	6
FEZF2	6
ATXN7	6
MITF	6
ZNF654	6
ZIC4	6
ZIC1	6
MSX1	6
NKX3-2	6
KLF3	6

NFKB1	6
LEF1	6
MEF2C	6
NR2F1	6
EGR1	6
EBF1	6
TFAP2A	6
ID4	6
ATF6B	6
RXRB	6
TEAD3	6
BACH2	6
POU3F2	6
SIM1	6
HIVEP2	6
PLAGL1	6
UNCX	6
FOXK1	6
ZNF316	6
SP8	6
CREB5	6
GLI3	6
DLX5	6
FOXP2	6
ZNF800	6
EGR3	6
EBF2	6
ZNF703	6
KAT6A	6
ST18	6
BHLHE22	6
HEY1	6
ZNF704	6
ZNF706	6
ZHX1	6
SCRT1	6
GLIS3	6
DMRTA1	6
ZBTB5	6
NR4A3	6
LHX2	6
ZEB1	6
ARID5B	6
ZNF503	6
VAX1	6
EMX2	6
EBF3	6
SOX6	6
PAX6	6

ZBTB16	6
NR4A1	6
ZNF385A	6
NEUROD4	6
RFX4	6
FOXN4	6
SMAD9	6
SOX1	6
FOXG1	6
NPAS3	6
ELMSAN1	6
MEIS2	6
SMAD3	6
SKOR1	6
ARNT2	6
ZNF774	6
NR2F2	6
ZNF843	6
ZFHX3	6
FOXC2	6
FOXL1	6
CAMTA2	6
HES7	6
SOX9	6
ONECUT2	6
TSHZ1	6
RFX2	6
ZNF333	6
ZNF536	6
ZNF599	6
ZNF382	6
FOSB	6
MEIS3	6
ZNF808	6
ZNF264	6
ZSCAN1	6
ZNF584	6
ZNF132	6
EBF4	6
INSM1	6
ZNF337	6
MAFB	6
TSHZ2	6
SIM2	6
PPARA	6
ARX	6
DACH2	6
ZMAT1	6
BHLHB9	6

ZNF75D	6
SOX3	6
MECP2	6